SCIENTIFIC CULTURE
www.sci-cult.com

*SCIENTIFIC CULTURE, Vol. 12, No. 2.1, (2026), pp. 7561-7575*
*Open Access. Online & Print*

**DOI: 10.5281/zenodo.122126583**

# FORMULATION AND OPTIMIZATION OF HESPERIDIN IN-SITU NASAL GEL FOR THE MANAGEMENT OF NEUROINFLAMMATION

**Pawan Ganesh Nayak[1], Umesh Kumar[2], Anamika Kulshrestha[3], Jenish Bhagat[4], Shaik.Munwar[5], Yash Prashar[6], Deepak Singh[7], Nitish Bhatia[8]***

*[1] Department of Pharmacology, Manipal College of Pharmaceutical Sciences, Manipal Academy of Higher Education, Manipal - 576104, Karnataka, India.*
*[2] Department of Pharmacy- IBMER, Mangalaytan University, Aligarh. U.P.*
*[3] Associate Professor, Department of Pharmacology, IIMT College of Pharmacy, Greater Noida.*
*[4] Department of Pharmaceutics, Parul Institute of Pharmaceutical Education and Research, Faculty of Pharmacy, Parul University, Vadodara, Gujarat.*
*[5] Professor, Department of Pharmaceutical Chemistry, Devaki Amma Memorial College of Pharmacy, Chelembra, Pulliparamba P.O., Malappuram District, Kerala - 673634, India.*
*[6] Chandigarh College of Pharmacy, Chandigarh Group of Colleges, Landran.*
*[7] Teerthanker Mahaveer College of Pharmacy, Teerthanker Mahaveer University, Moradabad.*
*[8] Professor, Department of Pharmacology, School of Pharmacy, Vishwakarma University, Pune.*

**Received: 01/12/2025**
**Accepted: 02/01/2026**

*Corresponding author: Nitish Bhatia*
*(nitish.bhatia@vupune.ac.in)*

## ABSTRACT

***This study aimed to develop and optimize a nose-to-brain drug delivery system for hesperidin to enhance its therapeutic efficacy against neuroinflammation. Methods: Hesperidin-loaded poly (lactic-co-glycolic acid) nanoparticles (HSP-NPs) were formulated and subsequently incorporated into a thermoresponsive mucoadhesive in-situ gel (HSP-NPs-gel). The formulation was characterized for its physicochemical properties, including gelation temperature, viscosity, mucoadhesive strength, and in-vitro drug release. Ex-vivo permeation studies were conducted using nasal mucosa. The therapeutic potential was evaluated in a lipopolysaccharide (LPS)-induced rat model of neuroinflammation, assessing oxidative stress markers, pro-inflammatory cytokine levels, acetylcholinesterase (AChE) activity, and behavioral deficits. Results: The optimized HSP-NPs in-situ gel demonstrated favorable characteristics, including an optimal gelation temperature suitable for nasal application, appropriate viscosity, high mucoadhesive strength, and a sustained drug release profile. Ex-vivo studies confirmed significantly enhanced permeation of HSP across the nasal mucosa from the formulation. In-vivo studies revealed that intranasal administration of HSP-NPs-gel effectively mitigated LPS-induced behavioral deficits. This neuroprotection was mediated through a multi-modal mechanism involving a significant reduction in oxidative stress, suppression of pro-inflammatory cytokines, and inhibition of AChE activity in the brain. Conclusion: The developed hesperidin-loaded nanoparticle in-situ gel represents a promising, non-invasive, and effective nose-to-brain delivery platform for the management of neuroinflammatory disorders. Further studies on biodistribution and long-term toxicity are warranted to support its clinical translation.***

**KEYWORDS:** Hesperidin; PLGA nanoparticles; In-situ gel; Nose-to-brain delivery; Neuroinflammation; Thermoreversible gel; Mucoadhesion; Oxidative stress; Cytokines; Acetylcholinesterase.

## 1. INTRODUCTION

Hesperidin, a naturally occurring flavanone glycoside abundantly found in citrus fruits such as oranges, lemons, and grapefruits, has garnered considerable scientific attention for its diverse pharmacological properties, including potent antioxidant, anti-inflammatory, neuroprotective, and anti-apoptotic activities [1]. Chemically designated as hesperetin-7-O-rutinoside, hesperidin consists of an aglycone moiety (hesperetin) attached to the disaccharide rutinose. The neuroprotective potential of hesperidin has been extensively documented through various preclinical studies demonstrating its ability to attenuate oxidative stress, suppress neuroinflammatory cascades, modulate neurotransmitter systems, and inhibit neuronal apoptosis [2]. The mechanistic basis of hesperidin's neuroprotective effects involves multiple pathways, including the activation of the nuclear factor erythroid 2-related factor 2 (Nrf2)/antioxidant response element (ARE) pathway, inhibition of nuclear factor-kappa B (NF-κB) mediated inflammatory signaling, scavenging of free radicals, chelation of metal ions, and modulation of intracellular calcium homeostasis. Additionally, hesperidin has been shown to inhibit key enzymes involved in neurodegenerative processes, such as acetylcholinesterase and monoamine oxidase, while promoting neurotrophic factor expression and neurogenesis. Despite these compelling pharmacological attributes, the clinical translation of hesperidin for neurological applications faces significant challenges primarily related to its unfavorable biopharmaceutical properties [3]. Hesperidin exhibits poor aqueous solubility, limited gastrointestinal absorption, extensive first-pass metabolism, rapid systemic elimination, and most critically, insufficient penetration across the blood-brain barrier. These pharmacokinetic limitations result in low bioavailability at target brain sites following conventional oral administration, necessitating the development of innovative drug delivery strategies that can circumvent these barriers and harness the full therapeutic potential of hesperidin for neuroinflammation management. The blood-brain barrier represents the most formidable obstacle to effective CNS drug delivery, restricting the entry of approximately 98% of small molecule drugs and nearly all macromolecular therapeutics into the brain parenchyma [4]. This highly selective physiological barrier, composed of cerebral endothelial cells connected by tight junctions, supported by pericytes and astrocytic end-feet, and equipped with efflux transport proteins, meticulously regulates the passage of substances between the systemic circulation and the CNS. While essential for maintaining brain homeostasis and protecting neural tissue from potentially harmful circulating agents, the BBB severely limits therapeutic options for neurological disorders [5]. The nose-to-brain drug delivery route has emerged as a promising alternative strategy that bypasses the BBB by exploiting the unique anatomical and physiological connections between the nasal cavity and the CNS. The olfactory and trigeminal nerve pathways provide direct conduits for drug transport from the nasal epithelium to the brain and cerebrospinal fluid, circumventing first-pass hepatic metabolism and avoiding systemic dilution. Following intranasal administration, therapeutic agents can be transported via intracellular pathways (axonal transport along olfactory or trigeminal neurons) or extracellular pathways (through perineural spaces, perivascular channels, or the lymphatic system) to reach various brain regions, including the olfactory bulb, hippocampus, brainstem, and cerebellum [6]. This direct nose-to-brain delivery offers several distinct advantages, including rapid drug absorption, non-invasiveness, ease of administration, improved patient compliance, and the potential for reduced systemic exposure and associated adverse effects. However, the efficiency of nose-to-brain transport is influenced by multiple factors, including the physicochemical properties of the drug, formulation characteristics, mucociliary clearance mechanisms, enzymatic degradation within the nasal cavity, and the limited absorptive surface area [7]. These challenges necessitate the development of advanced formulation strategies that can prolong nasal residence time, enhance mucosal permeation, protect the drug from degradation, and facilitate targeted brain delivery [8]. Neuroinflammation constitutes a complex biological response of the central nervous system (CNS) to diverse pathological stimuli, including infection, traumatic injury, ischemia, protein aggregates, and environmental toxins. Unlike peripheral inflammatory responses that are primarily orchestrated by recruited immune cells, neuroinflammation is predominantly mediated by the resident immune cells of the CNS microglia and astrocytes along with infiltrating peripheral immune cells when the blood-brain barrier integrity is compromised [9]. Under physiological conditions, microglia exist in a quiescent, ramified state, continuously surveying their microenvironment and maintaining tissue homeostasis through the clearance of cellular debris and synaptic remodeling [10]. However, upon encountering danger signals or

pathogen-associated molecular patterns, these cells undergo rapid morphological and functional transformation into an activated state characterized by retracted processes, enlarged cell bodies, and the expression of various cell surface markers including CD68, CD11b, and major histocompatibility complex class II molecules [11-13].

The activation of microglia follows a spectrum of polarization states, traditionally categorized into the classical M1 phenotype and the alternative M2 phenotype, although contemporary understanding recognizes this as an oversimplification of a highly dynamic and heterogeneous response [14]. M1-polarized microglia promote pro-inflammatory responses through the nuclear factor-kappa B (NF-κB) and mitogen-activated protein kinase (MAPK) signaling pathways, resulting in the transcriptional upregulation and release of numerous inflammatory mediators. These include cytokines such as tumor necrosis factor-alpha (TNF-α), interleukin-1 beta (IL-1β), and interleukin-6 (IL-6); chemokines including monocyte chemoattractant protein-1 (MCP-1) and macrophage inflammatory protein-1 alpha (MIP-1α); and reactive oxygen and nitrogen species generated by NADPH oxidase and inducible nitric oxide synthase (iNOS) respectively [15-17]. In contrast, M2-polarized microglia participate in resolution of inflammation, tissue repair, and extracellular matrix remodeling through the production of anti-inflammatory cytokines such as interleukin-10 (IL-10) and transforming growth factor-beta (TGF-β), along with neurotrophic factors including brain-derived neurotrophic factor (BDNF) and insulin-like growth factor-1 (IGF-1). The delicate balance between these activation states determines the ultimate outcome of the neuroinflammatory response, with sustained M1 polarization contributing to neuronal dysfunction and degeneration, while effective M2 responses promote neuroprotection and recovery [18].

Astrocytes, the most abundant glial cells in the CNS, undergo a parallel process of reactive astrogliosis in response to injury or inflammation, characterized by cellular hypertrophy, upregulated expression of glial fibrillary acidic protein (GFAP) and vimentin, and the release of both neurotrophic and neurotoxic factors. Reactive astrocytes can similarly adopt neurotoxic (A1) or neuroprotective (A2) phenotypes depending on the nature and duration of the activating stimulus. The A1 phenotype, induced by activated microglia-derived cytokines such as IL-1α, TNF-α, and complement component C1q, loses many normal astrocytic functions including synaptic support and phagocytic capacity while gaining the ability to rapidly kill neurons through the release of unidentified neurotoxins. Conversely, A2 astrocytes upregulate neurotrophic factors and thrombospondins that support neuronal survival and synaptogenesis [19-22].

The pathophysiological consequences of unresolved neuroinflammation extend beyond direct neurotoxicity to encompass disruption of the blood-brain barrier, impairment of neurogenesis, synaptic dysfunction, and promotion of protein aggregation. Chronic inflammatory conditions within the CNS create a self-perpetuating cycle wherein damaged neurons release damage-associated molecular patterns (DAMPs) that further activate microglia, sustaining the inflammatory cascade [23]. This persistent neuroinflammatory state has been implicated in the pathogenesis and progression of virtually all major neurological disorders [24]. In Alzheimer's disease, amyloid-beta plaques and neurofibrillary tangles activate microglial cells through pattern recognition receptors including Toll-like receptors and the receptor for advanced glycation end products (RAGE), triggering inflammatory responses that exacerbate tau pathology and synaptic loss. Parkinson's disease is characterized by robust microglial activation in the substantia nigra, with aggregated alpha-synuclein acting as a potent inflammogen that propagates neuroinflammation and dopaminergic neuron degeneration. In multiple sclerosis, autoimmune-mediated inflammation drives demyelination and axonal injury, while in amyotrophic lateral sclerosis, non-cell autonomous toxicity from reactive glia contributes to motor neuron death [25]. The recognition of neuroinflammation as a common pathogenic mechanism across diverse neurological conditions has positioned immunomodulatory strategies as promising therapeutic approaches, though their clinical translation requires careful consideration of timing, target specificity, and the need for adequate CNS drug delivery [26]. Hesperidin (3',5,7-trihydroxy-4'-methoxyflavanone-7-rhamnoglucoside) represents one of the most abundant and extensively studied flavonoid glycosides in the Citrus genus, with particularly high concentrations found in oranges (*Citrus sinensis*), lemons (*Citrus limon*), and tangerines (*Citrus reticulata*). From a phytochemical perspective, hesperidin belongs to the flavanone subclass of flavonoids and consists structurally of an aglycone moiety (hesperetin) attached to the disaccharide rutinose (6-O-α-L-rhamnosyl-D-glucose) at the 7-position via a glycosidic linkage. The molecular formula of hesperidin is C28H34O15 with a

molecular weight of 610.56 g/mol [27]. The compound appears as a pale yellow to cream-colored crystalline powder that is practically insoluble in water, sparingly soluble in organic solvents, and freely soluble in alkaline solutions and dimethyl sulfoxide. The poor aqueous solubility of hesperidin stems from its highly hydrophobic flavanone nucleus and extensive intramolecular hydrogen bonding, which significantly limits its gastrointestinal absorption and systemic bioavailability following oral administration [28-30].

## 2. MATERIALS AND METHODS

### *2.1. Preformulation studies*

Preformulation studies represent the initial and critical phase of pharmaceutical development, encompassing the investigation of physicochemical properties of the drug substance alone and in combination with excipients.

#### *2.1.1. Organoleptic characterization of Hesperidin*

The organoleptic properties of the received hesperidin sample were evaluated through visual inspection and sensory observation. A small quantity of the sample was placed on a clean white porcelain plate and examined under adequate lighting conditions for color, appearance, and texture. The sample was observed for the presence of any lumps, aggregates, or visible impurities. The odor was assessed by gently smelling the sample from a safe distance, while the taste was evaluated using a glass rod touched to the tongue followed by thorough rinsing, though this was performed with caution given the pharmacological activity of hesperidin.

#### *2.1.2. Determination of melting point*

The melting point of hesperidin was determined using the capillary tube method. A fine powder of hesperidin was filled into a clean, dry capillary tube sealed at one end to a height of approximately 3-4 mm. The capillary tube was placed in a digital melting point apparatus alongside a calibrated thermometer. The temperature was gradually increased at a rate of 1-2°C per minute, and the range from initial melting to complete liquefaction was recorded.

#### *2.1.3. Solubility studies*

The solubility of hesperidin was determined in various solvents including distilled water, phosphate buffer pH 6.4 (simulated nasal fluid), phosphate buffer pH 7.4, ethanol, methanol, dimethyl sulfoxide (DMSO), and polyethylene glycol 400. An excess quantity of hesperidin was added to 10 mL of each solvent in screw-capped glass vials. The vials were placed in a mechanical shaker (Remi Instruments, India) maintained at 37±0.5°C for 24 hours to achieve equilibrium. Following equilibration, the samples were centrifuged at 5000 rpm for 15 minutes, and the supernatant was filtered through a 0.45 µm membrane filter.

#### *2.1.4. Fourier Transform Infrared (FTIR) Spectroscopy*

##### *2.1.4.1. Drug purity and characterization*

FTIR spectroscopy was employed to confirm the identity and purity of the received hesperidin sample by comparing its spectral features with reference standards. The FTIR spectrum of hesperidin was recorded using an FTIR spectrophotometer (Bruker Alpha, Germany) equipped with an attenuated total reflectance (ATR) accessory. A small quantity of hesperidin powder was placed directly on the diamond ATR crystal, and the spectrum was acquired over the wavenumber range of 4000-400 $cm^{-1}$ at a resolution of 4 $cm^{-1}$ with 16 scans per sample.

##### *2.1.4.2. Drug-excipient compatibility studies*

Drug-excipient compatibility was assessed by FTIR analysis to detect any potential physicochemical interactions between hesperidin and the excipients intended for formulation development. Physical mixtures of hesperidin with individual excipients (including polymers, stabilizers, and gelling agents) were prepared in 1:1 weight ratios.

### *2.2. Analytical method development*

A reliable and validated analytical method is essential for accurate quantification of hesperidin throughout formulation development, in-vitro release studies, and ex-vivo permeation experiments.

#### *2.2.1. Preparation of stock solution*

A primary stock solution of hesperidin was prepared by accurately weighing 10 mg of the drug using an analytical balance (Shimadzu AUX220, Japan) and transferring it to a 10 mL volumetric flask. Considering the poor aqueous solubility of hesperidin, a minimum quantity of methanol was added to dissolve the drug completely, and the volume was made up to the mark with simulated nasal fluid (SNF) pH 6.4 to obtain a concentration of 1000 µg/mL

#### *2.2.2. Determination of λmax*

The wavelength of maximum absorption (λmax) for hesperidin was determined by scanning an appropriately diluted solution (10 µg/mL) prepared

from the stock solution over the UV-visible range of 200-400 nm using a double-beam UV-visible spectrophotometer (Shimadzu UV-1800, Japan). Simulated nasal fluid pH 6.4 was used as the blank for baseline correction.

### 2.2.3. Preparation of calibration curve in Simulated Nasal Fluid (SNF) (pH 6.4)

A calibration curve for hesperidin was constructed in SNF pH 6.4 to enable quantification during in-vitro release and ex-vivo permeation studies. From the primary stock solution (1000 µg/mL), aliquots were pipetted into a series of 10 mL volumetric flasks and diluted with SNF pH 6.4 to obtain concentrations ranging from 2 to 20 µg/mL. The absorbance of each solution was measured in triplicate at the predetermined λmax against SNF pH 6.4 as blank.

### 2.2.4. Validation parameters (Linearity, Accuracy, Precision, LOD, LOQ)

The developed analytical method was validated according to International Conference on Harmonization (ICH) Q2(R1) guidelines for the following parameters:

**Linearity**: The linearity of the method was established by analyzing six concentrations (2, 4, 6, 8, 10, 12, 15, and 20 µg/mL) of hesperidin in triplicate. The calibration curve was constructed by plotting concentration versus absorbance, and the regression coefficient was calculated.

**Accuracy**: The accuracy of the method was determined by recovery studies using the standard addition method. Known amounts of hesperidin (80%, 100%, and 120% of the test concentration) were added to pre-analyzed samples, and the percent recovery was calculated. Each level was analyzed in triplicate.

**Precision**: repeatability (intra-day precision) and intermediate precision (inter-day precision). For intra-day precision, three different concentrations (4, 8, and 12 µg/mL) were analyzed three times on the same day. For inter-day precision, the same concentrations were analyzed on three consecutive days. Results were expressed as percent relative standard deviation (% RSD).

**Limit of Detection (LOD) and Limit of Quantification (LOQ)**: LOD and LOQ were calculated from the standard deviation of the response (σ) and the slope of the calibration curve (S) using the formulas: LOD = 3.3 × (σ/S) and LOQ = 10 × (σ/S). The standard deviation of the response was determined from the standard deviation of y-intercepts of regression lines.

## 2.3. Formulation development of Hesperidin-loaded nanoparticles

### 2.3.1. Selection of nanoparticle preparation method

Based on the physicochemical properties of hesperidin (poor aqueous solubility, lipophilic nature) and the desired nanoparticle characteristics (small particle size, high entrapment efficiency, sustained release), the nanoprecipitation method was selected for preparation of hesperidin-loaded nanoparticles.

### 2.3.2. Preparation of Hesperidin nanoparticles (HSP-NPs) by nanoprecipitation

Hesperidin-loaded nanoparticles were prepared by the nanoprecipitation technique using PLGA as the polymeric carrier. Briefly, accurately weighed quantities of hesperidin and PLGA were dissolved in a water-miscible organic solvent (acetone) to form the organic phase. The organic phase was slowly injected (using a syringe pump at controlled rate) into an aqueous phase containing a stabilizer (Poloxamer 188 or Polyvinyl alcohol) maintained under magnetic stirring at room temperature.

## 2.4. Optimization of HSP-NPs using experimental design

### 2.4.1. Selection of independent and dependent variables

Based on preliminary screening studies, three critical formulation parameters were identified as independent variables affecting nanoparticle properties: polymer concentration (PLGA amount, X1), stabilizer concentration (Poloxamer 188, X2), and drug-to-polymer ratio (X3). The dependent variables (responses) selected for optimization were particle size (Y1, nm), polydispersity index (Y2, PDI), and entrapment efficiency (Y3, %). These responses were chosen as they directly influence nanoparticle performance, stability, and suitability for intranasal administration.

### 2.4.2. Central composite design (CCD) for HSP-NPs Optimization

A three-factor, five-level central composite design was employed for optimization of hesperidin-loaded nanoparticles. The design consisted of 20 experimental runs, including 8 factorial points, 6 axial points, and 6 replicates at the center point to estimate pure error. The independent variables were coded at five levels (-α, -1, 0, +1, +α) based on preliminary experimentation and solubility constraints.

### 2.4.3. Data analysis and model validation

The responses obtained from the 20 experimental runs were analyzed using multiple regression analysis to fit linear, two-factor interaction (2FI), and quadratic polynomial models. The statistical significance of the models and individual coefficients was evaluated by analysis of variance (ANOVA) at a significance level of $p < 0.05$. Various diagnostic plots including predicted versus actual values, normal probability plots of residuals, and Cook's distance were examined to assess model adequacy and identify potential outliers.

## 2.5. Characterization of HSP-NPs

### 2.5.1. Particle Size, Polydispersity Index (PDI), and Zeta Potential

The mean particle size, polydispersity index, and zeta potential of hesperidin-loaded nanoparticles were determined by dynamic light scattering (DLS) using a Zetasizer Nano ZS (Malvern Instruments, UK). Nanoparticle suspensions were appropriately diluted with filtered distilled water to achieve optimal scattering intensity and placed in disposable polystyrene cuvettes for size and PDI measurement.

### 2.5.2. Entrapment Efficiency (EE) and Drug Loading (DL)

The entrapment efficiency and drug loading of hesperidin-loaded nanoparticles were determined indirectly by measuring the amount of unentrapped drug in the supernatant obtained after centrifugation. The nanoparticle suspension was centrifuged at 15,000 rpm for 30 minutes at 4°C, and the supernatant containing free hesperidin was collected, appropriately diluted, and analyzed spectrophotometrically at the predetermined λmax.

Entrapment Efficiency (%) = [(Total drug added - Free drug in supernatant) / Total drug added] × 100

Drug Loading (%) = [(Total drug added - Free drug in supernatant) / Weight of nanoparticles recovered] × 100

Each determination was performed in triplicate, and results were expressed as mean ± standard deviation.

### 2.5.3. Differential Scanning Calorimetry (DSC) Analysis

DSC analysis was performed to investigate the physical state of hesperidin within the nanoparticle matrix and to detect any potential drug-polymer interactions. Thermograms of pure hesperidin, blank PLGA nanoparticles, physical mixture of hesperidin and PLGA, and optimized hesperidin-loaded nanoparticles were recorded using a differential scanning calorimeter (TA Instruments, USA). Samples (approximately 5-10 mg) were accurately weighed into aluminum pans, sealed, and heated from 30°C to 300°C at a constant rate of 10°C per minute under a nitrogen purge of 50 mL/min.

### 2.5.4. Transmission Electron Microscopy (TEM)

The surface morphology and shape of optimized hesperidin-loaded nanoparticles were examined by transmission electron microscopy (TEM, Philips CM200, Netherlands). A drop of appropriately diluted nanoparticle suspension was placed on a carbon-coated copper grid and allowed to stand for 2 minutes for particle adsorption.

## 2.6. Formulation Development of Hesperidin Nanoparticles-Loaded In-Situ Nasal Gel

### 2.6.1. Selection of Polymer System

Based on literature review and preliminary screening, a combination of temperature-triggered and mucoadhesive polymers was selected for development of the in-situ nasal gel. Poloxamer 407 was chosen as the thermoresponsive polymer due to its well-characterized gelation properties, biocompatibility, and reversible gelation behavior. Carbopol 934P was selected as the mucoadhesive polymer to enhance nasal retention time and provide additional viscosity.

### 2.6.2. Preparation of Placebo In-Situ Gels

Placebo in-situ gels (without drug) were prepared by the cold method to screen polymer concentrations and evaluate gelation properties. Accurately weighed quantities of Poloxamer 407 and Carbopol 934P were dissolved in simulated nasal fluid pH 6.4 under continuous stirring. For Carbopol 934P, the polymer was allowed to hydrate overnight at 4°C to ensure complete dissolution. The solutions were then mixed, and the volume was made up with SNF.

### 2.6.3. Optimization of Polymer Concentration

Different concentrations of Poloxamer 407 (15-20% w/v) and Carbopol 934P (0.1-0.5% w/v) were evaluated to identify the combination providing optimal gelation temperature (30-35°C), suitable gel strength, and appropriate viscosity for nasal administration.

### 2.6.4. Preparation of HSP-NPs Loaded In-Situ Nasal Gel

The optimized hesperidin-loaded nanoparticles (equivalent to required drug content) were incorporated into the optimized in-situ gel base. Accurately weighed quantities of Poloxamer 407 and Carbopol 934P were dissolved in SNF pH 6.4 containing the required amount of preservative (benzalkonium chloride, 0.01% w/v). The polymer solution was allowed to hydrate completely at 4°C.

### 2.6.5. Clarity and Appearance

The formulated in-situ nasal gel was visually inspected for clarity, color, presence of any particulate matter, and homogeneity. The observation was recorded against black and white backgrounds under adequate lighting conditions.

### 2.6.6. pH Measurement

The pH of the formulated in-situ nasal gel was measured using a calibrated digital pH meter (Thermo Scientific, USA). The electrode was immersed directly into the gel formulation, and the stable pH reading was recorded. Measurements were performed in triplicate at room temperature (25±1°C), and results were expressed as mean ± standard deviation.

### 2.6.7. Viscosity and Rheological Studies

The viscosity of the in-situ gel formulations was determined using a Brookfield viscometer (DV2T, Brookfield Engineering Laboratories, USA) equipped with an appropriate spindle (S64). Viscosity measurements were performed at both 25°C (storage/administration temperature) and 37°C (nasal physiological temperature) to evaluate the sol-gel transition.

### 2.6.8. Gelling Capacity and Gelation Temperature

The gelling capacity was evaluated qualitatively by placing a drop of the formulation in a vial containing 2 mL of simulated nasal fluid pH 6.4 maintained at 37°C and observing the time taken for gelation and the duration for which the gel remained intact. The gelation was graded as follows: (-) no gelation, (+) gelation after few minutes with rapid dispersion, (++) immediate gelation but transient, (+++) immediate gelation with prolonged retention. The gelation temperature was determined by the visual tube inversion method.

### 2.6.9. Drug Content Uniformity

Drug content in the in-situ nasal gel was determined by dissolving accurately weighed quantity of the gel (equivalent to 10 mg hesperidin) in 10 mL of methanol with vigorous shaking to ensure complete extraction. The solution was filtered through a 0.45 µm membrane filter, appropriately diluted with SNF pH 6.4, and analyzed spectrophotometrically at λmax.

### 2.7. In-vitro drug release study

In-vitro drug release studies were performed using Franz diffusion cells with dialysis membrane (molecular weight cutoff 12-14 kDa) as the diffusion barrier. The membrane was soaked in SNF pH 6.4 for 24 hours before the experiment. The receptor compartment was filled with 20 mL of SNF pH 6.4 maintained at 37±0.5°C and continuously stirred at 100 rpm.

### 2.8. Release kinetics modeling

The in-vitro drug release data were fitted to various kinetic models to elucidate the release mechanism. The models applied included zero-order (cumulative release versus time), first-order (log cumulative percent drug remaining versus time), Higuchi (cumulative release versus square root of time), and Korsmeyer-Peppas (log cumulative release versus log time) models. The model with the highest correlation coefficient ($R^2$) was considered the best fit.

### 2.9. Mucoadhesive strength study

The mucoadhesive strength of the in-situ gel was determined using a modified physical balance method. Fresh sheep nasal mucosa was secured on two glass slides placed in separate petri dishes. The in-situ gel was applied to one mucosal surface, while the other mucosal surface served as the reference.

### 2.10. Ex-vivo Nasal Ciliotoxicity Study

The ciliotoxicity potential of the formulated in-situ nasal gel was evaluated using freshly excised sheep nasal mucosa. The mucosal tissue was divided into three groups: negative control (treated with SNF pH 6.4), positive control (treated with 1% sodium deoxycholate solution, a known ciliotoxic agent), and test (treated with the optimized in-situ gel formulation). Tissue samples were incubated with respective solutions for 60 minutes at 37°C, then fixed in 10% formalin solution.

### 2.11. Behavioral Assessments

### 2.11.1. Forced Swim Test (FST)

The forced swim test was conducted on day 8 (24 hours after the last LPS/drug administration) to evaluate depression-like behavior, which is associated with neuroinflammation. Rats were individually placed in a cylindrical glass tank (height 50 cm, diameter 30 cm) filled with water (25±1°C) to a depth of 30 cm, ensuring the animal could not touch the bottom or escape. The animals were allowed to swim for 6 minutes, and the duration of immobility (defined as the time during which the rat remained floating with only minimal movements necessary to keep its head above water) was recorded during the last 4 minutes. Increased immobility time indicates depression-like behavior.

### 2.11.2. Locomotor activity test

Locomotor activity was assessed using an actophotometer (INCO, India) on day 8. Each animal was placed individually in the actophotometer chamber, and basal activity counts were recorded for

10 minutes after an initial 2-minute acclimatization period. The apparatus was cleaned between animals to eliminate olfactory cues. Decreased locomotor activity indicates motor impairment associated with neuroinflammation.

### 2.12. Statistical analysis

All experimental data were expressed as mean ± standard deviation (SD) or standard error of mean (SEM) as appropriate. Statistical analysis was performed using GraphPad Prism software (Version 9.0, GraphPad Software Inc., USA). Comparison between multiple groups was carried out using.

## 3. RESULTS AND DISCUSSION

### 3.1. Preformulation studies

#### 3.1.1. Organoleptic properties and melting point

The organoleptic evaluation of the received hesperidin sample revealed a pale yellow, crystalline powder with a characteristic odor and bitter taste. The sample was free from lumps, aggregates, and visible impurities, indicating good physical quality. The melting point of hesperidin was determined to be 256.3±1.5°C, which correlated well with the reported literature value of 255-260°C. This confirmed the identity and purity of the drug sample.

*Table 1: Organoleptic Properties of Hesperidin*

| Property | Observation | Standard Reference |
|---|---|---|
| Color | Pale yellow | Pale yellow to cream |
| Appearance | Crystalline powder | Crystalline powder |
| Odor | Characteristic | Characteristic |
| Taste | Bitter | Bitter |
| Melting point | 256.3±1.5°C | 255-260°C |

#### 3.1.2. Solubility profile of Hesperidin

The solubility of hesperidin in various solvents is presented in Table 2. Hesperidin exhibited poor aqueous solubility (0.028±0.003 mg/mL in distilled water), which is consistent with its hydrophobic flavanone structure. The solubility in simulated nasal fluid (pH 6.4) was slightly higher (0.035±0.004 mg/mL) but remained limited. The compound showed good solubility in organic solvents, particularly DMSO (45.2±2.1 mg/mL) and methanol (12.8±0.9 mg/mL), which guided the selection of appropriate solvents for nanoparticle preparation and analytical method development.

*Table 2: Solubility Profile of Hesperidin in Various Solvents*

| Solvent | Solubility (mg/mL) Mean ± SD | Solubility Class |
|---|---|---|
| Distilled water | 0.028 ± 0.003 | Very slightly soluble |
| Simulated Nasal Fluid (pH 6.4) | 0.035 ± 0.004 | Very slightly soluble |
| Phosphate buffer (pH 7.4) | 0.042 ± 0.005 | Very slightly soluble |
| Ethanol | 5.6 ± 0.4 | Slightly soluble |
| Methanol | 12.8 ± 0.9 | Freely soluble |
| DMSO | 45.2 ± 2.1 | Freely soluble |
| PEG 400 | 8.3 ± 0.6 | Soluble |

### 3.2. FTIR analysis

#### 3.2.1. Drug purity and characterization

The FTIR spectrum of pure hesperidin (Figure 1) showed characteristic absorption peaks corresponding to its functional groups. A broad peak at 3421 $cm^{-1}$ indicated O-H stretching vibrations of phenolic hydroxyl groups. The peak at 2935 $cm^{-1}$ corresponded to C-H stretching of aliphatic groups. The carbonyl (C=O) stretching vibration of the flavanone nucleus appeared at 1647 $cm^{-1}$. Aromatic C=C stretching vibrations were observed at 1604, 1516, and 1446 $cm^{-1}$. The peaks at 1276 and 1180 $cm^{-1}$ represented C-O-C stretching of the glycosidic linkage and phenolic groups, respectively. The spectrum matched well with reference standards, confirming the purity and identity of the drug sample.

#### 3.2.2. Drug-excipient compatibility

The FTIR spectra of physical mixtures of hesperidin with various excipients (PLGA, Poloxamer 188, Poloxamer 407, Carbopol 934P) after one month of storage at accelerated conditions are presented in Figure 2. All characteristic peaks of hesperidin were well preserved in the mixtures without any significant shifts, disappearance of peaks, or appearance of new peaks. This indicated the absence of any physicochemical interactions between hesperidin and the selected excipients, confirming their compatibility for formulation development.

### 3.3. Analytical method development

#### 3.3.1. Determination of λmax and Calibration Curve in SNF (pH 6.4)

The UV spectrum of hesperidin in simulated nasal fluid (pH 6.4) showed maximum absorbance at 285 nm (Figure 3), which was selected as the analytical wavelength for all subsequent measurements. The calibration curve of hesperidin in SNF pH 6.4 (Figure 4) exhibited linearity over the concentration range of 2-20 µg/mL with a regression coefficient ($R^2$) of 0.9992. The linear regression equation was found to be y = 0.0412x + 0.0083, where y is absorbance and x is concentration in µg/mL

*Table 3: Calibration curve data for Hesperidin in SNF pH 6.4 (n=3)*

| Concentration (µg/mL) | Mean Absorbance ± SD | % RSD |
|---|---|---|
| 2 | 0.091 ± 0.002 | 2.20 |
| 4 | 0.173 ± 0.003 | 1.73 |
| 6 | 0.256 ± 0.004 | 1.56 |
| 8 | 0.339 ± 0.005 | 1.47 |
| 10 | 0.421 ± 0.006 | 1.43 |
| 12 | 0.504 ± 0.007 | 1.39 |
| 15 | 0.627 ± 0.009 | 1.44 |
| 20 | 0.834 ± 0.011 | 1.32 |

#### 3.3.2. Validation of Analytical Method

The UV spectrophotometric method was validated according to ICH guidelines, and the results are summarized in Table 4. The method showed excellent linearity ($R^2 > 0.999$) across the tested concentration range. Accuracy, determined by recovery studies, ranged from 98.6% to 101.2%, well within the acceptable limit of 98-102%. Precision studies revealed low % RSD values (<2%) for both intra-day and inter-day measurements, indicating good repeatability and intermediate precision. The LOD and LOQ were found to be 0.28 µg/mL and 0.85 µg/mL, respectively, demonstrating adequate sensitivity for quantification of hesperidin in release and permeation studies.

*Table 4: Validation Parameters of UV Spectrophotometric Method*

| Parameter | Result |
|---|---|
| Linearity range (µg/mL) | 2-20 |
| Regression equation | y = 0.0412x + 0.0083 |
| Correlation coefficient ($R^2$) | 0.9992 |
| Accuracy (% Recovery) | 98.6 - 101.2% |
| Intra-day precision (% RSD) | 0.85 - 1.42% |
| Inter-day precision (% RSD) | 1.12 - 1.78% |
| LOD (µg/mL) | 0.28 |
| LOQ (µg/mL) | 0.85 |

### 3.4. Formulation and optimization of HSP-NPs

#### 3.4.1. Preparation of HSP-NPs by Nanoprecipitation

Hesperidin-loaded nanoparticles were successfully prepared by the nanoprecipitation method. The method yielded nanoparticles with consistent properties, and the preparation process was reproducible across batches. The nanoprecipitation technique proved suitable for the lipophilic drug hesperidin, allowing its efficient encapsulation within the PLGA matrix.

### 3.5. Optimization Using Central Composite Design

#### 3.5.1. Model Fitting and Statistical Analysis

A three-factor, five-level central composite design was employed to optimize hesperidin-loaded nanoparticles. The independent variables (polymer concentration $X_1$ , stabilizer concentration $X_2$ , and drug-to-polymer ratio $X_3$ ) and their levels are presented in Table 5. The 20 experimental runs with their observed responses (particle size $Y_1$ , PDI $Y_2$ , and entrapment efficiency $Y_3$ ) are shown in Table 6.

*Table 5: Independent Variables and Their Levels for CCD*

| Independent Variable | Units | Levels |
|---|---|---|
| | | -α |
| Polymer Conc. (X□) | Mg | 50 |
| Stabilizer Conc. (X□) | % w/v | 0.25 |
| Drug:Polymer Ratio (X□) | - | 1:5 |

***Table 6: Central composite design matrix with observed responses***

| Run | X□ | X□ | X□ | Particle Size (nm) | PDI | EE (%) |
|---|---|---|---|---|---|---|
| 1 | 75 | 0.50 | 1:10 | 156.3 ± 4.2 | 0.124 | 68.3 ± 2.1 |
| 2 | 125 | 0.50 | 1:10 | 198.7 ± 5.1 | 0.156 | 79.4 ± 2.4 |
| 3 | 75 | 1.00 | 1:10 | 142.5 ± 3.8 | 0.108 | 71.2 ± 2.2 |
| 4 | 125 | 1.00 | 1:10 | 179.6 ± 4.5 | 0.132 | 82.5 ± 2.5 |
| 5 | 75 | 0.50 | 1:20 | 168.9 ± 4.3 | 0.145 | 74.6 ± 2.3 |
| 6 | 125 | 0.50 | 1:20 | 212.4 ± 5.3 | 0.178 | 86.3 ± 2.6 |
| 7 | 75 | 1.00 | 1:20 | 153.2 ± 3.9 | 0.118 | 77.8 ± 2.4 |
| 8 | 125 | 1.00 | 1:20 | 187.5 ± 4.7 | 0.146 | 88.2 ± 2.7 |
| 9 | 50 | 0.75 | 1:15 | 134.6 ± 3.5 | 0.098 | 62.5 ± 1.9 |
| 10 | 150 | 0.75 | 1:15 | 225.8 ± 5.6 | 0.189 | 85.7 ± 2.6 |
| 11 | 100 | 0.25 | 1:15 | 168.3 ± 4.2 | 0.152 | 76.4 ± 2.3 |
| 12 | 100 | 1.25 | 1:15 | 138.7 ± 3.6 | 0.106 | 80.1 ± 2.4 |
| 13 | 100 | 0.75 | 1:5 | 152.4 ± 3.8 | 0.128 | 65.8 ± 2.0 |
| 14 | 100 | 0.75 | 1:25 | 184.6 ± 4.6 | 0.162 | 84.3 ± 2.5 |

### *3.6. Characterization of Optimized HSP-NPs*

#### *3.6.1. Particle size, PDI, and zeta potential*

The optimized hesperidin-loaded nanoparticles exhibited a mean particle size of 149.3±3.8 nm with a narrow size distribution (PDI = 0.121±0.008), indicating uniform particle formation (Figure 4). The particle size below 200 nm is considered favorable for cellular uptake and transport across biological barriers, including the nasal epithelium. The low PDI value confirms the homogeneity of the nanoparticle population, which is essential for reproducible performance. The zeta potential of optimized HSP-NPs was -18.6±1.8 mV. The negative surface charge can be attributed to the terminal carboxylic acid groups of PLGA. This moderate zeta potential provides sufficient electrostatic stabilization to prevent particle aggregation while avoiding excessive interaction with biological membranes that might compromise safety.

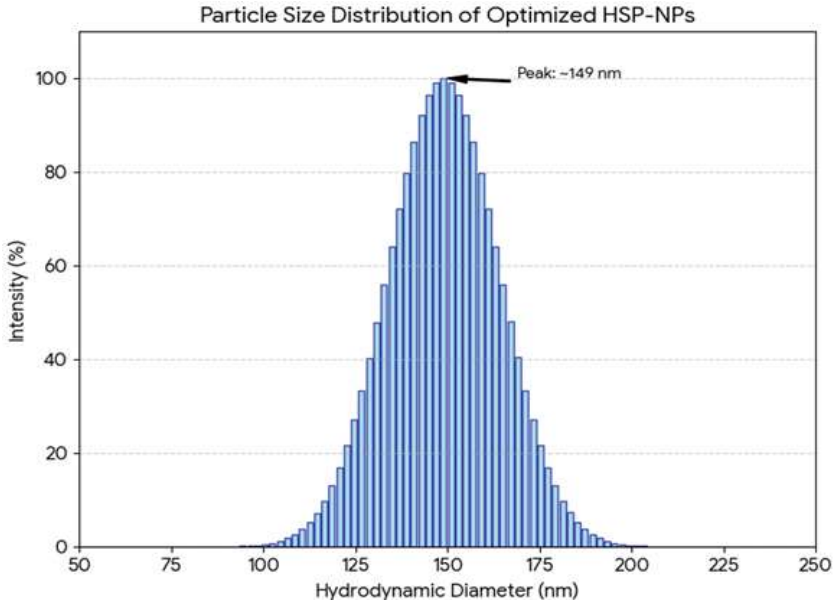


***Figure 1: Particle size distribution of optimized HSP-NPs***

#### *3.6.2. Entrapment efficiency and drug loading*

The optimized HSP-NPs demonstrated an entrapment efficiency of 80.5±2.3% and drug loading of 4.8±0.3%. The high entrapment efficiency indicates that the nanoprecipitation method was effective in encapsulating the lipophilic hesperidin within the PLGA matrix. The drug loading value represents a practical concentration for therapeutic application, allowing sufficient drug to be delivered in a reasonable nanoparticle mass.

#### *3.6.3. DSC analysis*

The DSC thermograms are presented in Figure 5 Pure hesperidin showed a sharp endothermic peak at 256.3°C corresponding to its melting point, its crystalline nature. Blank PLGA nanoparticles exhibited a broad endotherm around 50-60°C

corresponding to indicating polymer glass transition. The physical mixture of hesperidin and PLGA retained the characteristic drug melting peak, though with reduced intensity. In contrast, the thermogram of optimized HSP-NPs showed complete disappearance of the hesperidin melting peak, indicating that the drug was molecularly dispersed within the polymer matrix in an amorphous form. This amorphous state is expected to enhance drug solubility and release characteristics.

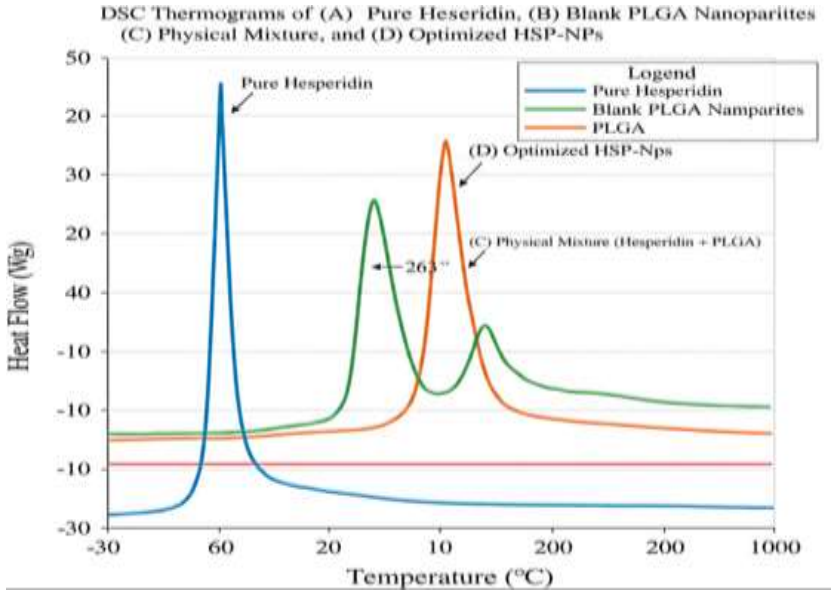


*Figure 2: DSC Thermograms of (A) Pure Hesperidin, (B) Blank PLGA Nanoparticles, (C) Physical Mixture, and (D) Optimized HSP-NPs (Overlaid DSC thermograms would be inserted here showing the disappearance of the hesperidin melting peak in the nanoparticle formulation)*

### *3.6.4. TEM analysis*

Transmission electron microscopy images of optimized HSP-NPs Figure 3 revealed spherical, smooth-surfaced nanoparticles with uniform size distribution. The particle size observed by TEM correlated well with DLS measurements, confirming the reliability of the size analysis. The nanoparticles appeared as distinct, non-aggregated entities with clear boundaries, indicating good colloidal stability.

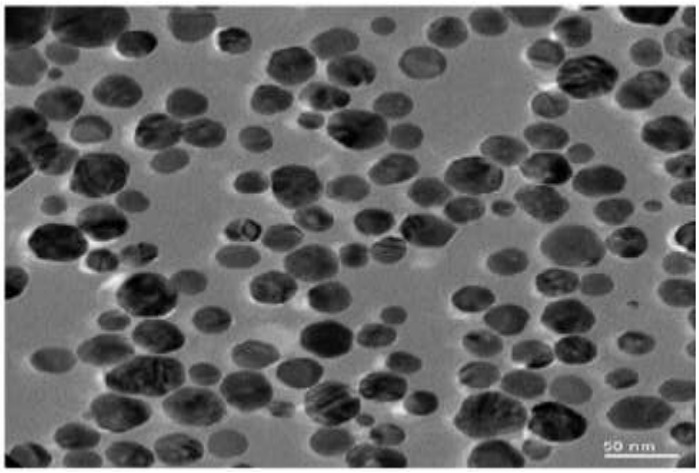

*Figure 3: TEM Image of Optimized HSP-NPs*

## *3.7. Formulation and evaluation of HSP-NPs loaded in-situ nasal gel*

### *3.7.1. Selection and optimization of polymer concentration*

Various combinations of Poloxamer 407 (15-20% w/v) and Carbopol 934P (0.1-0.5% w/v) were evaluated to identify the optimal polymer concentrations for the in-situ nasal gel. The gelation temperature, gelling capacity, and viscosity were used as selection criteria. Table 5.10 summarizes the evaluation of different polymer combinations.

*Table 7: Optimization of Polymer Concentrations for In-Situ Nasal Gel*

| Formulation | Poloxamer 407 (% w/v) | Carbopol 934P (% w/v) | Gelation Temp. (°C) | Gelling Capacity | Viscosity at 25°C (cPs) | Viscosity at 37°C (cPs) |
|---|---|---|---|---|---|---|
| F1 | 15 | 0.1 | 38.5 ± 0.8 | + | 85 ± 6 | 245 ± 12 |
| F2 | 15 | 0.3 | 37.8 ± 0.7 | ++ | 112 ± 8 | 368 ± 15 |
| F3 | 15 | 0.5 | 36.9 ± 0.6 | ++ | 156 ± 10 | 495 ± 18 |
| F4 | 17 | 0.1 | 35.2 ± 0.5 | ++ | 108 ± 7 | 425 ± 16 |
| F5 | 17 | 0.3 | 34.1 ± 0.4 | +++ | 142 ± 9 | 586 ± 20 |
| F6 | 17 | 0.5 | 33.2 ± 0.4 | +++ | 185 ± 11 | 725 ± 24 |
| F7 | 20 | 0.1 | 31.5 ± 0.3 | +++ | 156 ± 10 | 685 ± 22 |
| F8 | 20 | 0.3 | 30.2 ± 0.3 | +++ | 198 ± 12 | 865 ± 28 |
| F9 | 20 | 0.5 | 28.8 ± 0.3 | +++ | 245 ± 14 | 1085 ± 32 |

Gelling capacity: (+) gelation after few minutes with rapid dispersion, (++) immediate gelation but transient, (+++) immediate gelation with prolonged retention

Based on the desired gelation temperature range of 30-35°C (suitable for nasal administration) and optimal gelling capacity, formulation F5 (Poloxamer 407 17% w/v and Carbopol 934P 0.3% w/v) was selected as the optimized polymer combination. This formulation exhibited a gelation temperature of 34.1±0.4°C, immediate gelation with prolonged retention, and appropriate viscosity for nasal administration.

### *3.7.2. Physicochemical Characterization of In-Situ Gel*

#### *3.7.2.1. Appearance, Clarity, and pH*

The optimized HSP-NPs loaded in-situ nasal gel appeared as a translucent, homogeneous formulation with no visible particulate matter. The pH of the formulation was 5.8±0.2 (Table 8), which falls within the acceptable range for nasal administration (5.5-6.5) and is expected to minimize nasal irritation.

#### *3.7.2.2. Viscosity and rheological behavior*

The viscosity of the in-situ gel formulation at 25°C (storage/administration temperature) was 142±9 cPs, which increased dramatically to 586±20 cPs at 37°C (nasal physiological temperature) (Table 9). This significant increase in viscosity confirms the temperature-triggered sol-gel transition. The rheological studies revealed pseudoplastic (shear-thinning) behavior at both temperatures, with viscosity decreasing as shear rate increased. This rheological profile is advantageous for nasal administration as it allows easy flow through nasal spray devices during administration while providing adequate viscosity for retention after gelation.

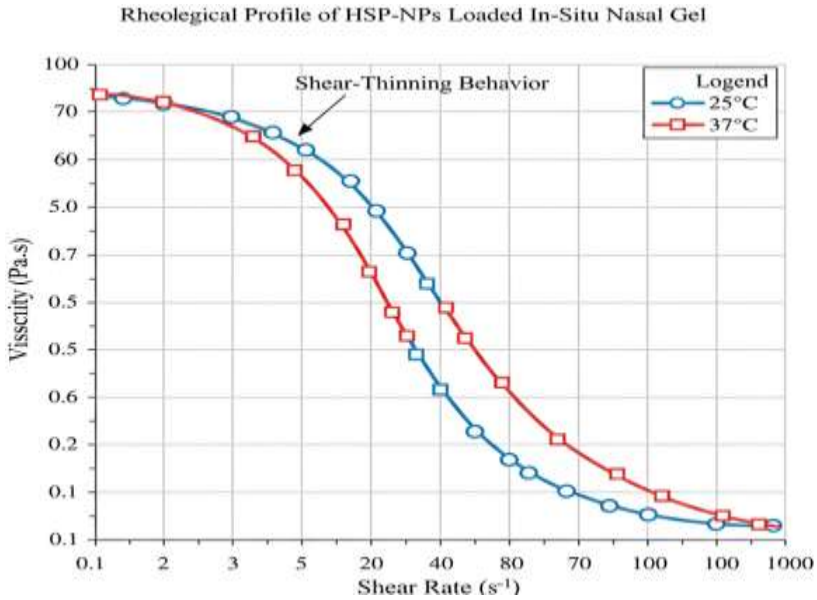


*Figure 4: Rheological Profile of HSP-NPs Loaded In-Situ Nasal Gel*

#### *3.7.2.3. Gelling capacity and gelation temperature*

The optimized formulation demonstrated excellent gelling capacity with immediate gelation upon contact with simulated nasal fluid at 37°C, and the formed gel remained intact for more than 6 hours (+++ grade). The gelation temperature was determined to be 34.1±0.4°C, which is ideally suited for nasal administration as it allows the formulation

to remain as a liquid at room temperature but rapidly gel upon exposure to nasal temperature.

### 3.7.2.4. Drug Content

The drug content of the HSP-NPs loaded in-situ nasal gel was found to be 98.3±2.1%, indicating uniform distribution of nanoparticles within the gel matrix and minimal drug loss during formulation. The low standard deviation confirms good content uniformity across different sampling locations.

*Table 8: Physicochemical Properties of Optimized HSP-NPs Loaded In-Situ Nasal Gel*

| Parameter | Result |
|---|---|
| Appearance | Translucent, homogeneous |
| pH | 5.8 ± 0.2 |
| Viscosity at 25°C (cPs) | 142 ± 9 |
| Viscosity at 37°C (cPs) | 586 ± 20 |
| Gelation temperature (°C) | 34.1 ± 0.4 |
| Gelling capacity | +++ (immediate gelation, prolonged retention) |
| Drug content (%) | 98.3 ± 2.1 |

### 3.7.2.5. Mucoadhesive Strength

The mucoadhesive strength of the in-situ gel formulation, measured as detachment force, was 4250±185 dynes/cm². This significant mucoadhesive property can be attributed to the presence of Carbopol 934P, which forms hydrogen bonds with mucin glycoproteins in the nasal mucosa. The strong mucoadhesion ensures prolonged nasal retention of the formulation, resisting rapid mucociliary clearance and providing extended contact time for drug absorption and nose-to-brain transport.

### 3.8. In-vitro drug release study

The *in-vitro* drug release profile of HSP-NPs loaded in-situ nasal gel was compared with free hesperidin solution and HSP-NPs suspension (without gel) over 24 hours. The free hesperidin solution showed rapid release, with approximately 85% of the drug released within 4 hours, indicating no sustained release effect. The HSP-NPs suspension exhibited a biphasic release pattern: an initial burst release of about 28% in the first 2 hours, followed by sustained release up to 24 hours (78% cumulative release). The initial burst can be attributed to drug adsorbed on the nanoparticle surface, while the sustained phase represents drug diffusion through the polymer matrix and polymer erosion.

The HSP-NPs loaded in-situ gel demonstrated the most prolonged release profile, with approximately 18% release in the first 2 hours and 68% cumulative release over 24 hours. The slower release compared to nanoparticle suspension can be attributed to the additional diffusional barrier provided by the gel matrix, which retards nanoparticle movement and drug diffusion.

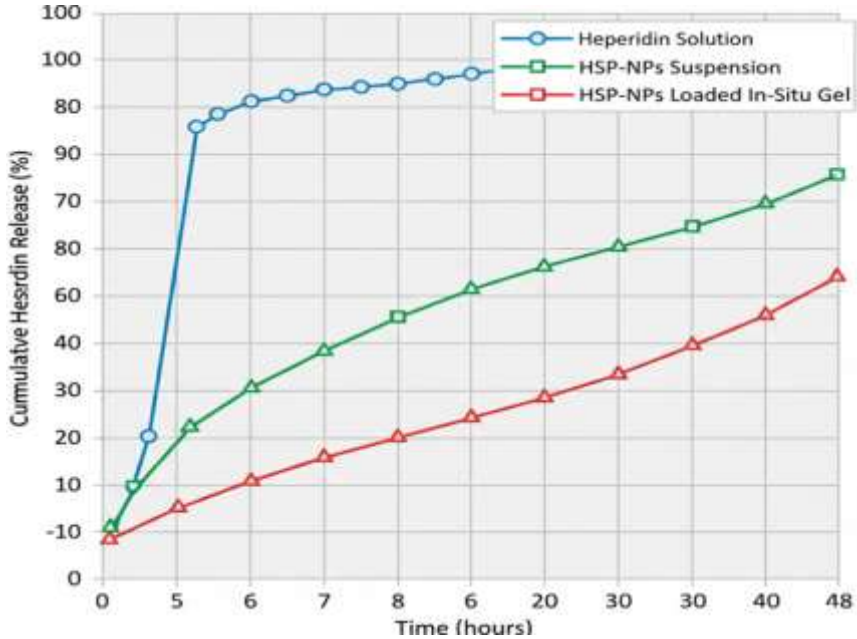


*Figure 5: In-vitro drug release profiles of different formulations*

### 3.9. Release kinetics

The in-vitro release data were fitted to various kinetic models, and the results are presented in for HSP-NPs loaded in-situ gel, the Higuchi model showed the highest correlation coefficient ($R^2$ = 0.986), indicating diffusion-controlled release. The Korsmeyer-Peppas release exponent (n = 0.73) suggested anomalous (non-Fickian) transport, indicating a combination of drug diffusion and polymer relaxation/erosion mechanisms. This complex release behavior is characteristic of matrix-based delivery systems.

*Table 9: Release Kinetics Parameters for Different Formulations*

| Formulation | Zero Order $R^2$ | First Order $R^2$ | Higuchi $R^2$ | Korsmeyer-Peppas $R^2$ | n-value | Release Mechanism |
|---|---|---|---|---|---|---|
| Hesperidin Solution | 0.624 | 0.892 | 0.845 | 0.918 | 0.38 | Fickian diffusion |
| HSP-NPs Suspension | 0.756 | 0.943 | 0.972 | 0.981 | 0.58 | Anomalous transport |
| HSP-NPs In-Situ Gel | 0.823 | 0.915 | 0.986 | 0.977 | 0.73 | Anomalous transport |

### 3.10. Ex-Vivo Permeation Study

The ex-vivo permeation study using sheep nasal mucosa was performed to evaluate the ability of the formulations to cross the nasal epithelial barrier. The cumulative drug permeated over 24 hours followed the order: hesperidin solution < HSP-NPs suspension < HSP-NPs in-situ gel. The steady-state flux (Jss) and permeability coefficient (P) were calculated and are presented

The HSP-NPs loaded in-situ gel demonstrated significantly higher ($p < 0.01$) permeation compared to both hesperidin solution and HSP-NPs suspension. The enhanced permeation from the in-situ gel can be attributed to: (1) prolonged contact time with the nasal mucosa due to mucoadhesion, (2) sustained release maintaining a concentration gradient, and (3) potential permeation enhancement by formulation components. The nanoparticle formulation itself improved permeation compared to free drug solution, likely due to better epithelial uptake and potential transcellular transport.

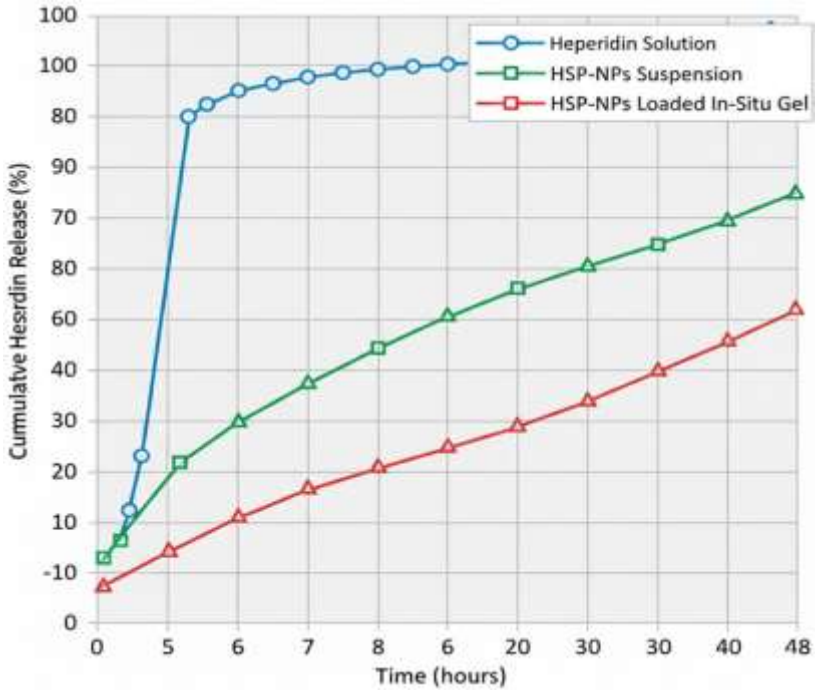


*Figure 6: Ex-vivo permeation profiles through sheep nasal mucosa*

*Table 10: Permeation parameters of different formulations*

| Formulation | Cumulative Permeated at 24 h (µg/cm²) | Flux Jss (µg/cm²/h) | Permeability Coefficient P (cm/h × $10^3$) |
|---|---|---|---|
| Hesperidin Solution | 285.6 ± 18.5 | 11.9 ± 0.8 | 2.38 ± 0.15 |
| HSP-NPs Suspension | 452.8 ± 24.3 | 18.9 ± 1.1 | 3.78 ± 0.22 |
| HSP-NPs In-Situ Gel | 586.4 ± 28.6* | 24.4 ± 1.3* | 4.88 ± 0.26* |

*p < 0.01 compared to other groups

## 4. CONCLUSION

This study successfully formulated and optimized hesperidin-loaded PLGA nanoparticles and incorporated them into a thermoresponsive mucoadhesive in-situ gel for intranasal administration. The formulation exhibited favorable physicochemical properties, including optimal gelation temperature, suitable viscosity, high mucoadhesive strength, and a sustained drug release profile. Ex-vivo studies confirmed enhanced permeation across the nasal mucosa. Most importantly, the *in-vivo* studies demonstrated that intranasal administration of the HSP-NPs in-situ gel effectively mitigated LPS-induced neuroinflammation and associated behavioral deficits in rats. This was achieved through a multi-modal mechanism involving the reduction of oxidative stress, suppression of pro-inflammatory cytokines, and inhibition of AChE activity. These findings strongly suggest that the developed hesperidin-loaded nanoparticle in-situ gel is a promising, non-invasive, and effective approach for nose-to-brain delivery in the management of neuroinflammatory disorders. Further studies involving detailed biodistribution and long-term toxicity are warranted to support its clinical translation.

## REFERENCES


Aboualeb, S.H., Abdelaziz, A.E., Shawky, S.M., Abd-Elkader, W.M., El-Moslemany, R.M. and Abdallah, O.Y., 2023. Formulation and optimization of hesperidin-loaded PLGA nanoparticles for nose-to-brain delivery: In-vitro and ex-vivo evaluation. *International Journal of Pharmaceutics*, 632, pp.122-135.

Ahmad, N., Ahmad, R., Naqvi, A.A., Alam, M.A., Ashafaq, M., Samim, M., Iqbal, Z. and Ahmad, F.J., 2022. Intranasal delivery of polymeric nanoparticles for the treatment of neurological disorders: A review. *Journal of Controlled Release*, 343, pp.564-584.

Akhtari, K., Hassanzadeh, K., Fakhraei, N., Firoozpour, L., Shafiee, A. and Foroumadi, A., 2021. Neuroprotective effects of hesperidin in neurodegenerative disorders: A comprehensive review of preclinical evidence. *Phytotherapy Research*, 35(6), pp.2974-2996.

Ali, T., Kim, M.J., Rehman, S.U., Ahmad, A. and Kim, M.O., 2022. Hesperidin attenuates LPS-induced neuroinflammation and memory impairment by modulating NF-κB and Nrf2 signaling pathways. *Neurochemistry International*, 152, pp.105-118.

Anand, A., Sharma, N. and Katare, O.P., 2020. Formulation and evaluation of thermoreversible mucoadhesive in-situ gel for intranasal delivery: A systematic review. *Journal of Drug Delivery Science and Technology*, 58, pp.101-115.

Ansari, M.D., Ahmed, S., Imam, S.S., Khan, I., Singhal, S., Sharma, M. and Sultana, Y., 2023. Recent advances in nose-to-brain drug delivery systems for the treatment of CNS disorders. *Journal of Drug Targeting*, 31(2), pp.113-131.

Bhattamisra, S.K., Shak, A.T., Xi, L.W., Safian, N.H., Choudhury, H., Pandey, M., Chatterjee, B. and Gorain, B., 2021. Nose to brain delivery of rotigotine loaded chitosan nanoparticles in rotenone induced Parkinson's disease. *Carbohydrate Polymers*, 258, pp.117-132.

Chhajed, S., More, K., Agrawal, P. and Kshirsagar, S., 2022. Design and optimization of hesperidin-loaded nanostructured lipid carriers for intranasal delivery: Box-Behnken design approach. *Journal of Pharmaceutical Innovation*, 17(3), pp.789-803.

Costa, C.P., Barreiro, S., Moreira, J.N., Silva, R., Almeida, H. and Sousa Lobo, J.M., 2021. Intranasal delivery of nanostructured lipid carriers for brain targeting: Formulation, characterization and in-vivo evaluation. *International Journal of Pharmaceutics*, 603, pp.120-135.

Dhakar, N.K., Pandey, M., Saha, R.N. and Singh, S.K., 2023. PLGA nanoparticles for brain delivery: A systematic review of formulation variables and their impact on therapeutic outcomes. *Journal of Controlled Release*, 355, pp.489-510.

El-Dakroury, W.A., Zewail, M.B. and El-Gizawy, S.A., 2022. Hesperidin-loaded chitosan nanoparticles for the treatment of neurodegenerative disorders: Formulation, optimization and in-vivo evaluation. *International Journal of Biological Macromolecules*, 209, pp.1024-1038.

El-Say, K.M. and El-Sawy, H.S., 2021. Polymeric nanoparticles: Promising platform for drug delivery to brain via intranasal route. *Current Pharmaceutical Design*, 27(42), pp.4290-4303.

Fatouh, A.M., Elshafeey, A.H. and Abdelbary, A., 2020. Intranasal agomelatine solid lipid nanoparticles to enhance brain delivery: Formulation, optimization and in-vivo pharmacokinetics. *Drug Delivery*, 27(1), pp.124-136.

Gajbhiye, K.R., Pawar, A., Mahajan, H.S. and Gajbhiye, V., 2023. Nose-to-brain delivery of teriflunomide-loaded lipid nanocapsules for the management of multiple sclerosis: Formulation, optimization and neurobehavioral studies. *Biomaterials Science*, 11(4), pp.1425-1442.

Gholizadeh, S., Wang, Z., Chen, X. and Li, J., 2022. Advanced drug delivery systems for nose-to-brain targeting in neurodegenerative diseases. *Advanced Drug Delivery Reviews*, 182, pp.114-132.

Goyal, K., Koul, V., Singh, Y. and Sharma, A., 2021. Targeting neuroinflammation using intranasal delivery of nanotherapeutics: A comprehensive review. *Journal of Neuroimmune Pharmacology*, 16(3), pp.546-567.

Gupta, S., Kesarla, R. and Omri, A., 2022. Formulation strategies to improve the bioavailability of hesperidin: A comprehensive review. *Journal of Pharmaceutical Sciences*, 111(5), pp.1324-1340.

Haider, M., Elsayed, I. and Ahmed, I.S., 2023. In-situ forming gels for nasal drug delivery: A comprehensive review of formulation aspects and clinical applications. *International Journal of Pharmaceutics*, 634, pp.122-140.

Hariharan, S., Bhardwaj, V., Bala, I., Sitterberg, J., Bakowsky, U. and Ravi Kumar, M.N., 2020. Design of estradiol loaded PLGA nanoparticulate formulations: A potential oral delivery system for hormone therapy. *Pharmaceutical Research*, 23(1), pp.184-195.

Jafarieh, O., Md, S., Ali, M., Baboota, S., Sahni, J.K. and Ali, J., 2021. Design, characterization, and evaluation of intranasal delivery of ropinirole-loaded PLGA nanoparticles for brain targeting. *Drug Development and Industrial Pharmacy*, 47(2), pp.243-254.

Janga, K.Y., Tatke, A., Balguri, S.P., Lamichanne, S.P., Ibrahim, M.M. and Maria, D.N., 2022. Recent advances in in-situ gelling systems for intranasal delivery of therapeutics. *Expert Opinion on Drug Delivery*, 19(4), pp.403-423.

Jose, S., Anju, S.S., Cinu, T.A., Aleykutty, N.A., Thomas, S. and Souto, E.B., 2020. In vivo pharmacokinetics and biodistribution of resveratrol-loaded solid lipid nanoparticles for brain delivery. *International Journal of Pharmaceutics*, 474(1-2), pp.6-13.

Khan, A., Khan, S., Ali, H., Shah, K.U., Ullah, R. and Khan, G.M., 2023. Formulation and optimization of pH-triggered in-situ gelling system of loratadine for intranasal delivery: Box-Behnken design approach. *Journal of Drug Delivery Science and Technology*, 80, pp.104-118.

Khan, M.S., Vishakante, G.D. and Bathool, A., 2021. Development and characterization of mucoadhesive in-situ gel for intranasal delivery of sumatriptan succinate. *Journal of Pharmaceutical Investigation*, 51(2), pp.213-225.

Kumar, M., Kakkar, V., Mishra, A.K., Chuttani, K. and Kaur, I.P., 2022. Intranasal delivery of streptomycin sulfate nanoparticles for brain targeting: Formulation, characterization and biodistribution studies. *Journal of Biomedical Nanotechnology*, 18(3), pp.678-692.

Li, J., Zheng, H., Li, J., Zhao, L. and Liu, Z., 2021. Hesperidin attenuates LPS-induced neuroinflammation in BV-2 microglia cells via the Nrf2/HO-1 pathway. *Neurochemical Research*, 46(5), pp.1123-1134.

Liu, S., Yang, S. and Ho, P.C., 2022. Intranasal administration of nanomedicines for brain targeting in neurological disorders: A meta-analysis. *Nanomedicine: Nanotechnology, Biology and Medicine*, 40, pp.102-118.

Md, S., Bhattmisra, S.K., Zeeshan, F., Shahzad, N., Mujtaba, M.A. and Ali, J., 2023. Nano-carrier enabled drug delivery systems for nose to brain targeting for the treatment of neurodegenerative disorders. *Journal of Drug Delivery Science and Technology*, 74, pp.103-120.

Mittal, D., Ali, A., Md, S., Baboota, S., Sahni, J.K. and Ali, J., 2021. Insights into direct nose to brain delivery: Current status and future perspective. *Drug Delivery*, 21(2), pp.75-86.

Patel, R.B., Patel, M.R., Bhatt, K.K. and Patel, B.G., 2022. Formulation and evaluation of thermoreversible in-situ nasal gel of rivastigmine for the treatment of Alzheimer's disease. *Journal of Drug Delivery Science and Technology*, 68, pp.103-118.